Substrate stiffness affects particle distribution pattern in a drying suspension droplet F

R. Iqbal (iD), Atsushi Matsumoto (iD), A. Sudeepthi, Amy Q. Shen (iD), and A. K. Sen (iD)

COLLECTIONS

F   This paper was selected as Featured

View Online   Export Citation   CrossMark

ARTICLES YOU MAY BE INTERESTED IN

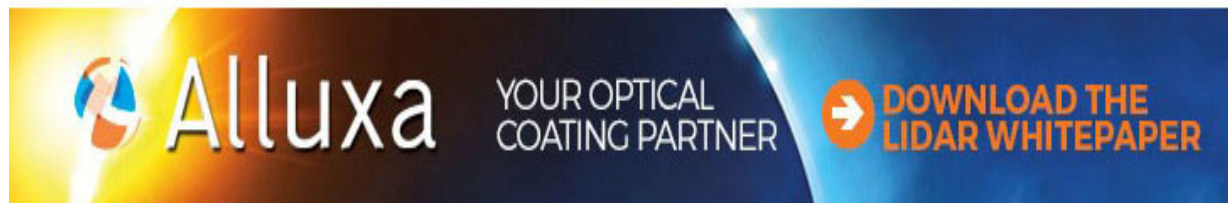Optical and electrical properties of two-dimensional palladium diselenide
Applied Physics Letters **114**, 253102 (2019); https://doi.org/10.1063/1.5097825

Microstructural heterogeneity drives reaction initiation in granular materials
Applied Physics Letters **114**, 254101 (2019); https://doi.org/10.1063/1.5108902

Real-time dynamic holographic display realized by bismuth and magnesium co-doped lithium niobate
Applied Physics Letters **114**, 241903 (2019); https://doi.org/10.1063/1.5107460

Substrate stiffness affects particle distribution pattern in a drying suspension droplet Ⓕ

R. Iqbal,[1] Ⓘ Atsushi Matsumoto,[2] Ⓘ A. Sudeepthi,[1] Amy Q. Shen,[2] Ⓘ and A. K. Sen[1,a] Ⓘ

AFFILIATIONS

[1]Microfluidics Laboratory, Department of Mechanical Engineering, Indian Institute of Technology Madras, Chennai 600036, India
[2]Micro/Bio/Nanofluidics Unit, Okinawa Institute of Science and Technology Graduate University, Okinawa 904-0412, Japan

[a]Author to whom correspondence should be addressed: ashis@iitm.ac.in

ABSTRACT

The complexities involved in achieving a tailor-made evaporative deposition pattern have remained a challenge. Here, we show that the morphological pattern of drying suspension droplets can be altered by varying substrate elastic modulus E. We find that the particle spot diameter and spacing between the particles scale with substrate stiffness as $d_s \sim E^{-0.15}$ and $s \sim E^{-1.23}$, respectively. We show that the larger spot diameter and spacing between particles on a softer substrate are attributed to a higher energy barrier U associated with stronger pinning of the contact line. The particle deposition pattern is characterized in terms of deposition index, I_d, whose value is <0.50 and >0.75 for centralized (multilayer) and uniform (monolayer) deposition patterns observed for stiffer and softer substrates, respectively. The outcome of the present study may find applications in biochemical characterization and analysis of micro-/nanoparticles.

Published under license by AIP Publishing. https://doi.org/10.1063/1.5097620

Droplet evaporation, apart from the association with the natural processes such as rain, fog, and dew, has found applications in inkjet printing,[1] spray cooling,[2] DNA microarrays,[3] biochemical assays,[4] and spraying of pesticides.[5] The topic has been extensively studied over the past two decades giving rise to important scientific advancements and technological developments.[6–9] Evaporation of particulate droplets involves rich physicochemical phenomena such as particle/particle interaction, particle/substrate interaction, patterning, and wetting. The seminal work by Deegan *et al.*[10] illustrated that an outwardly driven flow resulting from the differential evaporation flux drags micro-/nanoparticles toward the three-phase contact line, which gives rise to the accumulation of particles in the form of a ring, famously known as "the coffee-ring effect."

The coffee ring effect has been exploited in various applications such as detection of malaria and other biomarkers,[11,12] nanochromatography,[13] and disease diagnostics.[14] In contrast, the performance of matrix assisted laser deposition ionization spectrometry (MALDI),[15] surface enhanced Raman spectroscopy (SERS),[16] fluorescent microarrays,[17] and color filters in LCDs[18] is greatly hampered by this effect. Thus, an in-depth understanding of the kinetics of evaporation and the subsequent morphological pattern would have utmost importance for such applications. By varying the physicochemical parameters such as ambient pressure,[19] substrate temperature,[20,21] relative humidity,[22] substrate wettability,[23] properties of the solute (shape, size, and wettability)[24] and solvents (pH),[25] presence of the surfactants[26] and

additives,[27] and external flow fields,[28,29] the evaporation kinetics and hence the resulting deposition pattern can be controlled. However, the above strategies are either intrusive (e.g., use of additives and surfactants) or involve complicated procedures (compromising the shape of solute particles or composition of the liquid droplets) or external fields (i.e., electrowetting and acoustowetting).

While particles of a drying suspension droplet form coffee-ring patterns on hydrophilic substrates, they form centralized deposition patterns on hydrophobic substrates,[21] both of which are undesirable for various applications. The goal of this work is to examine the effect of substrate stiffness on the centralized deposition pattern observed on a hydrophobic substrate. Recent studies have revealed some of the effects of viscoelastic properties of substrates on the evaporation kinetics and particle deposition pattern.[30–32] It was found that water droplets over stiffer and softer substrates evaporate with CCA (constant contact angle) and CCR (constant contact radius) modes, respectively. Prolonged pinning and a larger contact radius on a softer substrate led to faster evaporation. Moreover, a smaller receding contact angle and a faster contact line velocity were observed on a softer substrate. For example, 2 μm silica particles inside a water-silica suspension droplet displayed craterlike (centralized) deposits with no particles at the rim over a stiffer substrate, while straight necklaces were shown aligned toward the rim over a softer substrate.

In the present work, we unravel the effect of substrate elasticity on the spot diameter and interdistance between particles. Using a

theoretical model, we explain that in the case of softer substrates, the observed larger spot diameter is attributed to a higher energy barrier, while the larger interdistance between particles is attributed to the enhanced elastic deformation. Using polystyrene particles of different sizes and concentrations and different drop volumes, we show that for increasingly softer substrates, the spot diameter increases and a transition from a centralized and multilayer deposition pattern to an unexpected uniform and monolayer deposition pattern is observed. Such a uniform and monolayer deposition pattern is difficult to achieve without direct compromise of liquid droplets (by either changing the shape of the microparticles or varying the pH of the solvents or adding the surfactants).[24–26] Finally, we introduce a dimensionless parameter "deposition index (I_d)" in order to predict and control the centralized or the uniform deposition pattern. Our results suggest that $I_d < 0.50$ results in centralized (multilayer) deposition patterns over stiffer substrates, while $I_d > 0.75$ results in uniform (monolayer) deposition patterns over softer substrates.

The schematic of the experimental setup is shown in Fig. S1 (Sec. S1). Clean glass substrates (thickness ∼1.1 mm, Matsunami, Japan) coated with a thin elastomeric layer (Sylgard 184, Dow Corning Toray, Japan) were used as the substrate for the experiments. To adjust elastic moduli of the substrate, crosslinkers were added to the base polymer at different ratios ranging from 10:1 to 50:1 and the cross-linked substrates are herein referred to as P10, P20, P30, P40, and P50. The ratio of the base polymer to the crosslinkers and the corresponding elastic modulus of the substrates are presented in Table S1. We performed experiments with suspension drops (DI water + polystyrene microparticles) of volume in the range of $0.5 - 2.0$ μl (maintaining $Bo \ll 1$) containing particles of size in the range of 0.2–6 μm at concentrations of 10^8–10^9 particles/ml, with a substrate contact angle of $113\pm10°$ and stiffness in the range of $E = 20 - 283$ kPa. For each experimental condition, identical experiments were repeated at least five times in order to establish the repeatability of the data and the error bars associated with the data are estimated from the standard deviation of the dataset. The materials and methods used for the fabrication of the substrates of different elastic moduli, preparation of the microbeads at different concentrations, and the experimental details are outlined in the supplementary material (see Sec. S1).

Figure 1(a) depicts the top and side views of the dried suspension droplets (of volume 1.0 μl, particle size 1.0 μm, concentration

10^9 particles/ml) on the different substrates (P10, P30, and P50) of elastic moduli 283, 120, and 20 kPa, respectively. The initial contact radius (just after dispense) of the suspension droplet is indicated by the dotted line in the top views. In all cases, owing to the hydrophobic nature of the substrates, instead of a coffee-ring, a centralized particle deposition pattern[23] is observed. The spot size was obtained from the gray scale intensity plot shown in Fig S2(a) (Sec. S2). The diameter of the dried particle spot was found to be much larger (864 ± 39 μm) for substrates of lower elastic modulus (i.e., P50 with $E = 20$ kPa) as compared to that (485 ± 35 μm) for a stiffer substrate (P10 with $E = 283$ kPa). Figure 1(b) shows the variation of the spot size with the substrate elastic modulus for different droplet volumes, particle sizes, and concentrations (also see Fig. S3). As observed, the particle spot diameter decreases with an increase in the substrate elastic modulus due to early receding of the contact line owing to a smaller energy barrier, which is discussed later. From the experimental data, the spot diameter is correlated with elastic modulus as $d_s \sim E^{-0.15}$ (with $R^2 = 0.95$).

In order to understand the contrasting morphological patterns on substrates of different elastic moduli, we looked into the evaporation dynamics. The variation of the contact radius $\hat{r}$ (r/r_o) and contact angle θ of drying suspension droplets (volume 1.0 μl, particle size 1 μm, concentration 10^9 particles/ml) with time $\hat{t}$ (t/t_E) on substrates of different elastic moduli ($E = 20 - 283$ kPa) is shown in Figs. 2(a) and S4(a) in the supplementary material. The contact radius r is normalized with respect to the initial contact radius r_0 (i.e., $\hat{r} = r/r_0$), and time scale t is normalized with respect to the corresponding evaporation time scale t_E (i.e., $\hat{t} = t/t_E$).

We observe that compared to a rigid substrate ($\hat{t}_p = 0.36$, $E = 283$ kPa), a droplet remains pinned over a much longer time ($\hat{t}_p = 0.94$) on a softer substrate, where $\hat{t}_p$ is the dimensionless time scale over which the contact line remains pinned. Since the contact line of a droplet remains pinned over a prolonged period of time on a softer substrate, the evaporation time scale t_E (which is inversely proportional to the contact radius)[32] was found to be lower for smaller substrate stiffness [see Fig. 2(b)]. From Fig. 2(a), over a time scale $t < \hat{t}_p$, when the contact line remains pinned, the contact angle decreases continuously and approaches the receding contact angle θ_r. For $\hat{t} > \hat{t}_p$, either the contact line recedes with a constant contact angle or both the contact radius and contact angle decrease simultaneously exhibiting a
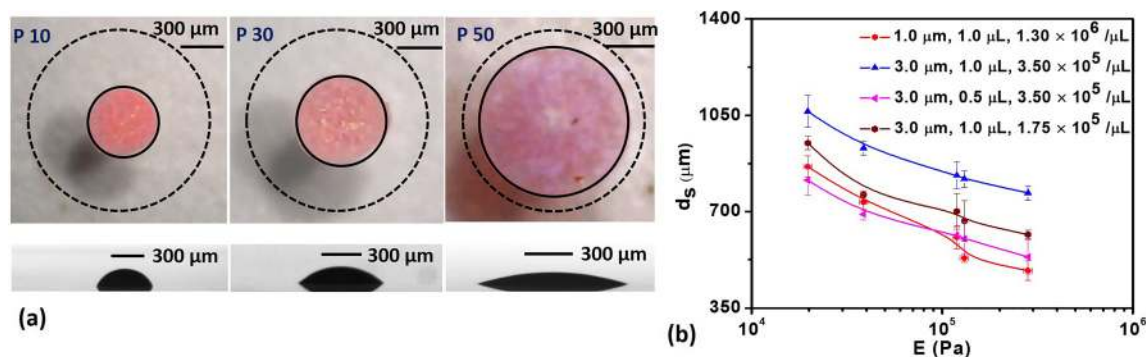

FIG. 1. (a) Differences in the morphological pattern (top and side views) of dried suspension droplets over P10 ($E \sim 283$ kPa), P30 ($E \sim 120$ kPa), and P50 ($E \sim 20$ kPa) substrates. (b) Variation of the spot diameter, d_s, with the substrate elastic modulus, G, for different droplet volumes, particle sizes, and concentrations.
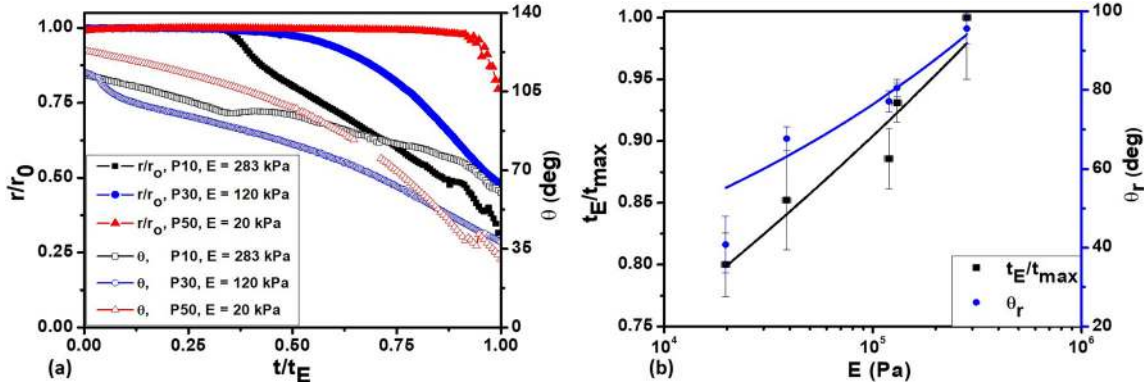
FIG. 2. (a) Variation of the normalized contact radius ($\hat{r} = r/r_0$) and contact angle (θ) over substrates of different elastic moduli: P10 ($E \sim 283$ kPa), P30 ($E \sim 120$ kPa), and P50 ($E \sim 20$ kPa), respectively. (b) Variation in the normalized evaporation time scale and the receding contact angle with the substrate elastic modulus, E.

mixed mode of evaporation. The variation of receding contact angle θ_r, with substrate elastic modulus E, is also depicted in Fig. 2(b) which shows that the receding angle θ_r scales with substrate elastic modulus E following $\theta_r \sim E^{0.20}$ (with $R^2 = 0.86$).

We see that in the case of a stiffer substrate ($E = 283$ kPa), the contact line recedes early ($\hat{t}_p = 0.36$), thus carrying the particles toward the center of the droplet giving rise to a much smaller particle spot diameter (485 μm) and particle deposition over multiple layers. On the other hand, in the case of a softer substrate ($E = 20$ kPa), pinning of the contact line over a significant part of the evaporation time scale ($\hat{t}_p = 0.94$) prevents migration of the particles toward the center, resulting in a much larger spot diameter (i.e., 863 μm) with distribution of particles in the form of a monolayer. Next, we employ a theoretical model to explain the above phenomena from the argument of free energy.

Droplets with Bond number, $Bo \ll 1$, take the shape of a spherical cap [Fig. 3(a)] due to the absence of the gravimetric flattening, and in that case, the droplet volume V and liquid/vapor interfacial area A can be expressed as

$$V = \frac{\pi r^3}{3 \sin^3 \theta}(1 - \cos\theta)^2(2 + \cos\theta), \quad A = \frac{2\pi r^2}{(1 + \cos\theta)}, \quad (1)$$

where r and θ are the contact radius and the contact angle of the droplet on a real surface, respectively. The Gibbs free energy G_b of the droplet arising from the interfacial energy components can be
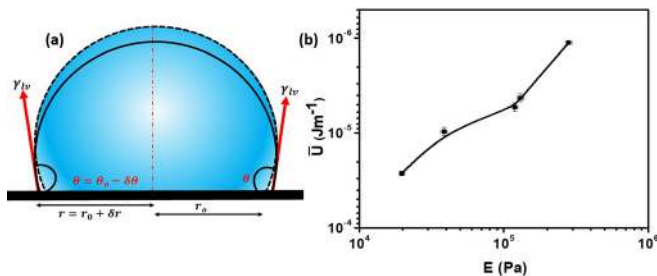

FIG. 3. (a) A schematic of the droplet over a hydrophobic substrate. The droplet over ideal and nonideal surfaces is denoted by the dotted and the solid line, respectively. (b) Variation of the potential energy barrier (per unit length), $\overline{U}$, with the substrate elastic modulus.

written as $G_b = \gamma_{LV}A + \pi r^2(\gamma_{SL} - \gamma_{SV})$, where γ_{LV}, γ_{SL}, and γ_{SV} are the liquid-vapor, solid-liquid, and solid-vapor interfacial tension values. Using the expression for the interfacial area from Eq. (1), we get

$$G_b = \gamma\pi r^2\left[\frac{2}{(1 + \cos\theta)} - \cos\theta_o\right], \quad (2)$$

where θ_o is the equilibrium contact angle of the droplet obtained from the Young's equation. Unlike an ideal surface, the droplet on a real/nonideal surface remains out of equilibrium due to surface asperities and chemical inhomogeneity.[33] Let the droplet be perturbed from its equilibrium state such that the modified contact radius becomes $r = r_o + \delta r$, and accordingly, the corresponding contact angle is $\theta = \theta_o - \delta\theta$, where r_o is the equilibrium contact radius [see Fig. 3(a)]. On an ideal surface, the contact angle of a liquid droplet corresponds to the Young's contact angle which remains constant, and the contact radius decreases during droplet evaporation. However, on a soft substrate, the surface asperities (see supplementary material Sec. S6), chemical inhomogeneity, and more importantly, the wetting ridge[34,35] together would offer an energy barrier U that prevents smooth receding of the contact line which remains pinned and only the contact angle decreases.

With the progress in evaporation, the volume of the droplet decreases, and thus, for a droplet pinned at the contact line, the contact angle decreases. This leads to a lack in capillary equilibrium, and the absence of capillary equilibrium is the source of excess free energy. Free energy of the nonequilibrated droplet can be obtained from the Taylor series expansion (and using the condition that the droplet is at equilibrium at $r = r_o$, thus, $\left(\frac{dG_b}{dr}\right)_{r=r_o} = 0$ and constant droplet volume $dV = 0$) as

$$\delta G_b \cong \left(\frac{d^2 G_b}{dr^2}\right)_{r=r_o}\frac{(\delta r)^2}{2} \cong \frac{2\pi r^2 \gamma_{LV}(\delta\theta)^2}{2(2 + \cos\theta_o)}, \quad (3)$$

where $\delta\theta$ is the difference between the actual contact angle (from the experiments, it decreases for a pinned droplet with the reduction in the volume during evaporation) and the corresponding equilibrium value θ_o. Taking θ_a as the actual contact angle at any time instant, we can write $\delta\theta = (\theta_o - \theta_a(t))$. Thus, we get

$$\delta G_b(t) \cong \left(\frac{d^2 G_b}{dr^2}\right)_{r=r_o} \frac{(\delta r)^2}{2} \cong \frac{2\pi r^2 \gamma_{LV}(\theta_o - \theta_a(t))^2}{2(2 + \cos\theta_o)}. \quad (4)$$

During the evaporation process, the actual contact angle θ_a decreases as time progresses, and thus, the excess Gibbs free energy δG_b increases with time. The variation in the excess Gibbs free energy δG_b with the actual contact angle, θ_a, which is a function of time t, for different substrate stiffness, is shown in Fig. S5. As observed, when the contact angle attains the receding contact angle θ_r, the excess Gibbs free energy attains the maximum value, i.e., $\delta G_{\max}$, which overcomes the energy barrier U and the contact line recedes. Using the previous equation, the maximum excess Gibbs free energy per unit length of the contact line $\overline{\delta G_{\max}}$ or the energy barrier $\overline{U}$ is obtained as

$$\overline{U} = \overline{\delta G_{\max}} = \frac{1}{2\pi r} \times \frac{2\pi r^2 \gamma_{LV}(\theta_o - \theta_r)^2}{2(2 + \cos\theta_o)}. \quad (5)$$

From the above equation, we plot the variation of maximum excess free energy $\overline{\delta G_{\max}}$ or the energy barrier $\overline{U}$ with substrate elastic modulus E [see Fig. 3(b)]. As observed, the energy barrier $\overline{U}$ is higher for a softer substrate ($E = 20$ kPa), and thus, the contact line remains pinned for a much longer duration of time $\hat{t}_p$ until the receding contact angle θ_r is attained. The higher energy barrier explains why a suspension droplet remains pinned for a longer time on a softer substrate, yielding a more homogeneous particle distribution pattern.

SEM images of the morphological patterns of the particles with substrates of elastic moduli 283 kPa and 20 kPa are depicted in Fig. 4(a) [also see in Figs. S6(a) and S6(b)], respectively. As observed, in the case of a rigid substrate, particles get deposited in closely packed multiple layers, whereas loosely packed, homogeneous, uniform monolayer particle deposition is observed in the case of a softer substrate. Also, in contrast to the rigid substrate in which the particles are packed closely, the interdistance (s) between the particles is found to be higher in the case of a softer substrate ($E = 20$ kPa) as compared to that for a stiffer substrate ($E = 283$ kPa). The hexagonal polygons obtained from the Voronoi diagram[36] for both substrates [inset of Figs. 4(a) and S6] show the ordered arrangements of the particles. In the case of the stiffer substrate, apart from the hexagonal polygons,

other polygons in square, rhombohedral, and random shapes lead to the disorder in the pattern. The optical profilometry results (see Fig. S7) suggest a disklike pattern and uniform pattern for the stiffer and softer substrates, respectively. The variation in the interparticle distance (s) with substrate elastic modulus E for different particle sizes is presented in Fig. 4(b). From the data, the interparticle distance correlates with the substrate elastic modulus as $s \sim E^{-1.23}$.

For an evaporative suspension droplet, to predict and control either the formation of a multilayer centralized deposition pattern or the formation of a uniform monolayer deposition pattern, we investigated the influence of the suspension droplet volume (V), size and concentration of the microparticles (a and C), surface tension (γ) of the liquid, and the substrate elastic modulus (E) on the evaporative deposition pattern of the suspension droplet. To consider the combined effect of the above parameters, we introduced a dimensionless parameter (see Sec. S5 in the supplementary material), "deposition index" $I_d = \left(\frac{d_s}{2r}\right) = \frac{0.33 a (CV)^{0.54} (\gamma/Ea)^{0.21}}{[(8/\pi)Vf(\theta)]^{\frac{1}{3}}}$, which is the ratio of the final deposition contact diameter (d_s) after the complete evaporation of the droplet to the initial (maximum) contact diameter of the droplet ($2r$) when dispensed, where $f(\theta) = \frac{3\sin^3\theta}{[(1-\cos\theta)^2(2+\cos\theta)]}$ is indicative of the contribution of the contact angle on the volume of the spherical cap (droplet). For a fixed droplet volume V, the initial contact line diameter $2r$ is obtained from Eq. (1), and the final deposition contact diameter (d_s) is obtained from fitting of the data presented in Figs. 1(b) and S3.

Moreover, with a very diluted suspension droplet, a monolayer along with a centralized deposition pattern can also be achieved due to the lack of the adequate number of particles. Thus, to achieve both uniform and monolayer deposition patterns, the particle concentration (i.e., number of particles per unit volume) should be on the order of a critical value given as $C_{crit} \approx \frac{P.F.[2.5Vf(\theta)]^{\frac{2}{3}}}{a^2 V}$ (see details in the supplementary material), where P.F. is the maximum packing fraction (which is 0.74 for spherical particles in a hexagonal arrangement). For the droplet volume in the range of 0.5–2 μl and the particle size in the range of 0.2–6 μm, the critical concentration $C_{crit} \sim 10^5$ to 10^6 per μl.

Figure 5 depicts the variation of I_d with E, for different particle sizes and droplet volumes. It is observed that for a particle size of 1 μm
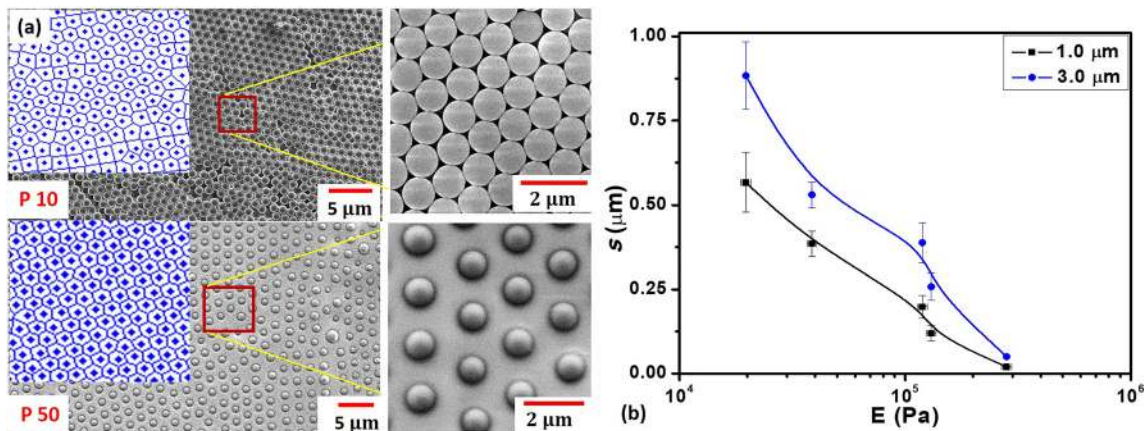

FIG. 4. (a) Differences in the morphological pattern obtained under SEM for (a) stiffer ($E \sim 283$ kPa) and softer ($E \sim 20$ kPa) substrates; particle size 1 μm. (b) Variation of the interparticle distance (s), with the substrate elastic modulus, E, for two different particle sizes, 1 and 3 μm, respectively.
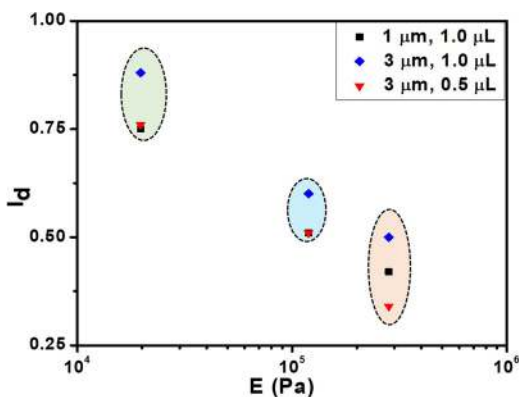
FIG. 5. Variation of deposition index, I_d, with E for different particle sizes and droplet volumes and a particle concentration of $10^6/\mu$l.

and concentration $10^6/\mu$l (which is $\geq C_{crit}$) presented in Fig. 2(a), the value of I_d is calculated to be 0.41 for the P10 and 0.75 for the P50 substrates, in agreement with the nonuniform (and multilayers) and uniform (and monolayer) deposition patterns observed in the case of P10 and P50 substrates, respectively. From the entire range of particle sizes and volumes studied here, with particle concertation $\geq C_{crit}$, it was observed that in order to obtain a uniform deposition pattern, the deposition index $I_d \sim 0.75$–0.85, whereas $I_d \sim 0.25$–0.50 would yield a nonuniform deposition pattern. Thus, to obtain best results in characterization and analysis of particles for biological and analytical applications, with other parameters fixed, appropriate substrate stiffness should be chosen to ensure large values of I_d.

In summary, we reported the role of the substrate elastic modulus in the particle distribution pattern in a drying suspension droplet. We observed that the particle spot diameter and interparticle distance can be controlled by simply varying the substrate elastic modulus. The outcome of the present study is relevant for ensuring a uniform and monolayer particle deposition pattern for the characterization and analysis of microparticles via analytical techniques.

See the supplementary material for the experimental details, rheological characterization, detailed evaporation kinetics morphological patterns under SEM, and optical profilometry.

REFERENCES

[1] B.-J. de Gans and U. S. Schubert, Langmuir **20**, 7789 (2004).
[2] C. Wang, R. Xu, Y. Song, and P. Jiang, Int. J. Heat Mass Transfer **112**, 279 (2017).
[3] M. Schena, D. Shalon, R. W. Davis, and P. O. Brown, Science **270**, 467 (1995).
[4] S. Weidner, P. Knappe, and U. Panne, Anal. Bioanal. Chem. **401**, 127 (2011).
[5] Y. Yu, H. Zhu, J. M. Frantz, M. E. Reding, K. C. Chan, and H. E. Ozkan, Biosyst. Eng. **104**, 324 (2009).
[6] H. Hu and R. G. Larson, J. Phys. Chem. B **106**, 1334 (2002).
[7] A.-M. Cazabat and G. Guéna, Soft Matter **6**, 2591 (2010).
[8] H. Y. Erbil, Adv. Colloid Interface Sci. **170**, 67 (2012).
[9] D. Brutin and V. Starov, Chem. Soc. Rev. **47**, 558 (2018).
[10] R. D. Deegan, O. Bakajin, T. F. Dupont, G. Huber, S. R. Nagel, and T. A. Witten, Nature **389**, 827 (1997).
[11] J. R. Trantum, D. W. Wright, and F. R. Haselton, Langmuir **28**, 2187 (2012).
[12] J. T. Wen, C.-M. Ho, and P. B. Lillehoj, Langmuir **29**, 8440 (2013).
[13] T.-S. Wong, T.-H. Chen, X. Shen, and C.-M. Ho, Anal. Chem. **83**, 1871 (2011).
[14] D. Brutin, B. Sobac, B. Loquet, and J. Sampol, J. Fluid Mech. **667**, 85 (2011).
[15] O. Kudina, B. Eral, and F. Mugele, Anal. Chem. **88**, 4669 (2016).
[16] W. Wang, Y. Yin, Z. Tan, and J. Liu, Nanoscale **6**, 9588 (2014).
[17] R. Blossey and A. Bosio, Langmuir **18**, 2952 (2002).
[18] Y.-C. Lin, Y.-Y. Lin, D. S. H. Wong, T.-J. Liu, S.-H. Wen, and K.-T. Huang, J. Appl. Polym. Sci. **120**, 1555 (2011).
[19] A. Askounis, K. Sefiane, V. Koutsos, and M. E. R. Shanahan, Colloids Surf., A **441**, 855 (2014).
[20] M. Parsa, S. Harmand, K. Sefiane, M. Bigerelle, and R. Deltombe, Langmuir **31**, 3354 (2015).
[21] N. D. Patil, P. G. Bange, R. Bhardwaj, and A. Sharma, Langmuir **32**, 11958 (2016).
[22] V. H. Chhasatia, A. S. Joshi, and Y. Sun, Appl. Phys. Lett. **97**, 231909 (2010).
[23] R. Iqbal, B. Majhy, A. Q. Shen, and A. K. Sen, Soft Matter **14**, 9901 (2018).
[24] P. J. Yunker, T. Still, M. A. Lohr, and A. G. Yodh, Nature **476**, 308 (2011).
[25] R. Bhardwaj, X. Fang, P. Somasundaran, and D. Attinger, Langmuir **26**, 7833 (2010).
[26] T. Still, P. J. Yunker, and A. G. Yodh, Langmuir **28**, 4984 (2012).
[27] L. Cui, J. Zhang, X. Zhang, L. Huang, Z. Wang, Y. Li, H. Gao, S. Zhu, T. Wang, and B. Yang, ACS Appl. Mater. Interfaces **4**, 2775 (2012).
[28] D. Mampallil, J. Reboud, R. Wilson, D. Wylie, D. R. Klug, and J. M. Cooper, Soft Matter **11**, 7207 (2015).
[29] H. B. Eral, D. M. Augustine, M. H. G. Duits, and F. Mugele, Soft Matter **7**, 4954 (2011).
[30] Y. S. Yu, Z. Q. Wang, and Y. P. Zhao, Acta Mech. Sin. **29**, 799 (2013).
[31] M. C. Lopes and E. Bonaccurso, Soft Matter **9**, 7942 (2013).
[32] M. C. Lopes and E. Bonaccurso, Soft Matter **8**, 7875 (2012).
[33] M. Oksuz and H. Y. Erbil, J. Phys. Chem. C **118**, 9228 (2014).
[34] S. J. Park, B. M. Weon, J. S. Lee, J. Lee, J. Kim, and J. H. Je, Nat. Commun. **5**, 4369 (2014).
[35] A. Carre and M. E. R. Shanahan, Langmuir **11**, 3572 (1995).
[36] Á. G. Marín, H. Gelderblom, D. Lohse, and J. H. Snoeijer, Phys. Rev. Lett. **107**, 085502 (2011).